Spatial distribution of water level impact to back-barrier bays

Alfredo L. Aretxabaleta[1], Neil K. Ganju[1], Zafer Defne[1], and Richard P. Signell[1]

[1] U.S. Geological Survey, Woods Hole, Massachusetts, 02543, USA

5   *Correspondence to*: Alfredo L. Aretxabaleta (aaretxabaleta@usgs.gov)

Abstract. Water level in semi-enclosed bays, landward of barrier islands, is mainly driven by offshore sea level fluctuations that are modulated by bay geometry and bathymetry, causing spatial variability in the ensuing response (transfer). Local wind setup can have a secondary role that depends on wind speed, fetch, and relative orientation of the wind direction and

10   the bay. Inlet geometry and bathymetry primarily regulate the magnitude of the transfer between open ocean and bay. Tides and short-period offshore oscillations are more damped in the bays than longer-lasting offshore fluctuations, such as storm surge and sea level rise. We compare observed and modeled water levels at stations in a mid-Atlantic bay (Barnegat Bay) with offshore water level proxies. Observed water levels in Barnegat Bay are compared and combined with model results from the Coupled Ocean-Atmosphere-Wave-Sediment Transport (COAWST) modeling system to evaluate the spatial

15   structure of the water level transfer. Analytical models based on the dimensional characteristics of the bay are used to combine the observed data and the numerical model results in a physically consistent approach. Model water level transfers match observed values at locations inside the Bay in the storm frequency band (transfers ranging from 70-100%) and tidal frequencies (10-55%). The contribution of frequency-dependent local setup caused by wind acting along the bay is also considered. The approach provides transfer estimates for locations inside the Bay where observations were not available

20   resulting in a complete spatial characterization. The approach allows for the study of the Bay response to alternative forcing scenarios (landscape changes, future storms, and rising sea level). Detailed spatial estimates of water level transfer can inform decisions on inlet management and contribute to the assessment of current and future flooding hazard in back-barrier bays and along mainland shorelines.

25   **Copyright statement**

1 Introduction

Back-barrier bays or coastal lagoons are common features along the coast of the United States. Their depths are usually on the order of a few meters and their horizontal extents are on the order of several tens of kilometers. They are often

30   surrounded by highly populated areas and susceptible to intense human and environmental stressors. During storms, surge and larger than normal waves combine to inundate low-elevation areas, resulting in hazards to coastal communities. Both hurricanes and winter storms affect coastal populations, infrastructure, and natural resources along the coastal bays of the United States (Nicholls et al., 2007).

Hazard assessments consist of a characterization of the spatial and temporal extent of damaging physical events and the determination of the specific characteristics of those events (Ludwig et al., 2018). While flooding in the mainland side of back-barrier bays has severe socio-economic implications, most of the coastal hazard evaluations (Gornitz et al., 1994; Thieler and Hammar-Klose, 1999; Klein and Nicholls, 1999; Kunreuther et al., 2000) have focused in open-coast areas.

5 Vulnerability evaluation of coastal areas around back-barrier bays requires extensive knowledge of the main hazard sources and their physical controls.

Water level in the bays is mainly driven by offshore sea level fluctuations with smaller effects by local wind and wave setups. The bay exchange with the ocean usually occurs through narrow inlets. The size of the inlet determines the frictional effects and the amount of dampening offshore fluctuations encounter (Keulegan, 1967). Tides and short-period offshore

10 oscillations tend to be more dampened in the bays than longer-lasting offshore fluctuations, such as storm surge and sea level rise.

Bay water level fluctuations are linked to offshore forcing especially at low frequencies, while wind acting directly over the bay is more connected to current fluctuations in the bay (Garvine, 1985). Chuang and Swenson (1981) determined that water level changes at subtidal frequencies in Lake Pontchartrain were controlled by coupled coastal ocean-bay fluctuations. Wong

15 and Wilson (1984) studied subtidal sea level fluctuations in Great South Bay and again found them primarily driven by bay-shelf coupling. In Delaware Bay, a bay-inlet system with a relatively large opening, Wong and DiLorenzo (1988) showed that remote effects dominate over local effects and that fluctuations at both tidal and subtidal frequencies in connected bays of the Delaware Bay system were forced by shelf sea level.

More recently, Aretxabaleta et al. (2014) analyzed water level data in Barnegat Bay and Great South Bay before and after

20 Hurricane Sandy and demonstrated that the offshore-bay transfer was not significantly altered by the geomorphologic changes caused by the storm. Aretxabaleta et al. (2017) described observed changes in both tidal amplitude and bay water level transfer from offshore in Great South Bay and connected bays and related the changes to the dredging of nearby inlets and the changing size of a breach across Fire Island caused by Hurricane Sandy. They also introduced an analytical model, based on the Chuang and Swenson (1981) approach but extended to interconnected bays, that incorporated bay and inlet

25 dimensions and matched the observed transfer of offshore water level fluctuations into the bay system.

In this study, we combine an analysis of observed water levels in Barnegat Bay with the results of numerical models and an analytical description of the system to characterize the spatial characteristics of the bay response to offshore fluctuations. The observations provide detailed information at five locations in the bay, while the numerical simulations can expand the analysis to the entire bay system. The analytical model allows for the evaluation of the importance of the dominant factors

30 affecting water level in bays. The combined approach can be used to provide consistent spatial maps of offshore water level impact into back-barrier bays. The method will be useful for coastal hazard assessment assisting in the management of nuisance flooding and providing spatial differences in vulnerability to perigean spring tides (king tides) and planning for flooding in response to storms of different durations. The final hazard estimates will be included as part of the U.S. Geological Survey Coastal Change Hazard portal (USGS, 2018).

2. Regional description

Barnegat Bay –Little Egg Harbor (BBLEH) estuary is a back-barrier bay along the coast of New Jersey (Figure 1). It is a shallow (average depth around 1.5 m) bay connected to the ocean through three openings: Little Egg Inlet in the south, Barnegat Inlet in the center, and Point Pleasant Canal, which is a much smaller connection in the north of the bay. Offshore

5   tidal amplitudes decrease slightly from 0.7 m in northern New York Bay to 0.6 m in central New Jersey. The southern sub-embayment (Little Egg Harbor) is more connected with the open ocean with tidal amplitudes ranging between 0.2 and 1 m, while the northern part (Barnegat Bay) has less exchange and tidal amplitudes are smaller than 0.2 m (Chant, 2001; Defne and Ganju, 2015).

3. Observational and model data

10   Water level observations from five stations in the BBLEH system (Table 1) and from two coastal stations are used to determine transfer from ocean to bay. The bay stations started recording in October 2007, while Sandy Hook and Atlantic City are long-term NOAA water level stations operational since 1910 and 1911, respectively (Table 1). Wind observations were obtained from the NDBC buoy 44065 (New York Harbor Entrance) for the period 2008-2018.

We used numerical simulations of Barnegat Bay for the period March-September 2012 (Defne and Ganju, 2015) and

15   October-December 2012 to obtain the spatial character of the water level response. The simulations used the Coupled Ocean Atmospheric Wave Sediment Transport modeling system (COAWST; Warner et al., 2010). The model resolution ranged from 40 m to 200 m, with the higher resolution located near complex geometry and around the inlets. The model is forced at the boundaries with tides from the ADCIRC tidal database for the western North Atlantic Ocean (Szpilka et al., 2016) and open-ocean forcing from subtidal water level and velocity from the ESPreSSO model (Wilkin and Hunter, 2013;

20   http://www.myroms.org/espresso/) and COAWST US east coast forecast (Warner et al., 2010; https://catalog.data.gov/dataset/coawst-forecast-system-usgs-us-east-coast-and-gulf-of-mexico-experimentalf9168). Defne and Ganju (2015) showed the model solution had sufficient skill to characterize bay dynamics under normal and storm conditions.

The impact in the bay of offshore forcing can be evaluated spectrally by estimating transfer functions in frequency space

25   between observed water levels offshore (input) and in the bays (output). The transfer functions are calculated using a Hanning window with over-lapping (50%) data segments with a length of 29 days to provide estimates near the main tidal frequencies (Aretxabaleta et al., 2017). The uncertainty envelopes for the transfer function are estimated using the Bendat and Piersol (1986) formulation.

4 Analytical Water Level Models

4.1 Offshore Impact on Bay Model

The impact of ocean sea level fluctuations in the bay can be explored with an analytical model of a generic bay system (Figure 2) consisting of multiple interconnected sub-embayments connected to the offshore by three separate inlets: Little

5 Egg Inlet, Barnegat Inlet, and Point Pleasant Canal. The model assumes that the bay water level responds as a level surface in each sub-embayment to ocean fluctuations, as local forcing in the bay is not included. The formulation is an extension of the approach proposed by Chuang and Swenson (1981) for a single inlet connecting to a bay and expanded by Wong and DiLorenzo (1988) to two connected bays and to multiple bays and inlets by Aretxabaleta et al. (2017). An analytical solution can be found for the entire system with expressions for all the connections in the system. The model solves the along-

10 channel depth-averaged momentum equation based on the balance between frictional effects and the elevation gradient between offshore and bay and the continuity equation for the bay/channel system based on the changing volume of the bays as water flows through the inlets. The model also allows the estimation of the effect of the breach in Mantoloking during Hurricane Sandy. An analytical solution can be found by dividing the entire system into 5 sub-embayments (based on constrictions inside the bay system) resulting in a system of equations that includes 13 equations and unknowns.

$$
\frac{\partial}{\partial t}
\begin{pmatrix} u_1 \\ u_2 \\ u_3 \\ u_4 \\ u_5 \\ u_6 \\ u_7 \\ u_8 \end{pmatrix}
= g
\begin{pmatrix} 1/L_1 \\ 1/L_2 \\ 1/L_3 \\ 1/L_4 \\ 1/L_5 \\ 1/L_6 \\ 1/L_7 \\ 1/L_8 \end{pmatrix}
\begin{pmatrix} \eta_o \phi_{LEI} - \eta_1 \\ \eta_1 - \eta_2 \\ \eta_2 - \eta_3 \\ \eta_o \phi_{BI} - \eta_3 \\ \eta_3 - \eta_4 \\ \eta_4 - \eta_5 \\ \eta_o \phi_{breach} - \eta_5 \\ \eta_o \phi_{PPC} - \eta_5 \end{pmatrix}
-
\begin{pmatrix} u_1 r_1 / h_1 \\ u_2 r_2 / h_2 \\ u_3 r_3 / h_3 \\ u_4 r_4 / h_4 \\ u_5 r_5 / h_5 \\ u_6 r_6 / h_6 \\ u_7 r_7 / h_7 \\ u_8 r_8 / h_8 \end{pmatrix}
$$

$$
\begin{pmatrix} A_1 \\ A_2 \\ A_3 \\ A_4 \\ A_5 \end{pmatrix}
\frac{\partial}{\partial t}
\begin{pmatrix} \eta_1 \\ \eta_2 \\ \eta_3 \\ \eta_4 \\ \eta_5 \end{pmatrix}
=
\begin{pmatrix} h_1 W_1 u_1 - h_2 W_2 u_2 \\ h_2 W_2 u_2 - h_3 W_3 u_3 \\ h_3 W_3 u_3 + h_4 W_4 u_4 - h_5 W_5 u_5 \\ h_5 W_5 u_5 - h_6 W_6 u_6 \\ h_6 W_6 u_6 + h_7 W_7 u_7 + h_8 W_8 u_8 \end{pmatrix}
$$

where g is the gravitational acceleration, A_m is the surface area of sub-embayment m; η_m the sea level in the m sub-embayment; η_o the sea level in the ocean; with h_n the water depth; W_n the width; L_n the length, and r_n the linear drag coefficient of channel n. ϕ_{LEI}, ϕ_{BI}, ϕ_{breach}, ϕ_{PPC} are the relationships between the water levels at offshore proxy stations (Sandy Hook or Atlantic City) and the water level just offshore of Little Egg Inlet, Barnegat Inlet, the breach at Mantoloking

5   caused by Sandy, and Point Pleasant Canal.

Assuming $\eta = \eta e^{i\omega t}$ and $u = u e^{i\omega t}$, then we can define $K_n = \dfrac{h_n W_n g}{L_n\left(\frac{r_n}{h_n}+i\omega\right)}$ for n=1 ,..., 8

then with the proper rearrangement, it yields:

$$\eta_3 = \frac{K_4\eta_o\phi_{BI} + \dfrac{\dfrac{K_1K_2K_3\eta_o\phi_{LEI}}{i\omega A_1 + K_1 + K_2}}{i\omega A_2 + K_2 + K_3 - \dfrac{K_2K_2}{i\omega A_1 + K_1 + K_2}} + \dfrac{\dfrac{K_5K_6(K_7\phi_{breach} + K_8\phi_{PPC})\eta_o}{i\omega A_5 + K_6 + K_7 + K_8}}{i\omega A_4 + K_5 + K_6 - \dfrac{K_6K_6}{i\omega A_5 + K_6 + K_7 + K_8}}}{i\omega A_3 + K_3 + K_4 + K_5 - \dfrac{K_3K_3}{i\omega A_2 + K_2 + K_3 - \dfrac{K_2K_2}{i\omega A_1 + K_1 + K_2}} - \dfrac{K_5K_5}{i\omega A_4 + K_5 + K_6 - \dfrac{K_6K_6}{i\omega A_5 + K_6 + K_7 + K_8}}}$$

The solution for the water level of the central sub-embayment can be used to recursively calculate the solutions for the rest

10   of the sub-embayments:

$$\eta_2 = \frac{K_3\eta_3 + \dfrac{K_2K_1\eta_o\phi_{LEI}}{i\omega A_1 + K_1 + K_2}}{i\omega A_2 + K_2 + K_3 - \dfrac{K_2K_2}{i\omega A_1 + K_1 + K_2}}$$

$$\eta_4 = \frac{K_5\eta_3 + \dfrac{K_6(K_7\phi_{breach} + K_8\phi_{PPC})\eta_o}{i\omega A_5 + K_6 + K_7 + K_8}}{i\omega A_4 + K_5 + K_6 - \dfrac{K_6K_6}{i\omega A_5 + K_6 + K_7 + K_8}}$$

$$\eta_1 = \frac{K_1\eta_o\phi_{LEI} + K_2\eta_2}{i\omega A_1 + K_1 + K_2}$$

$$\eta_5 = \frac{(K_7\phi_{breach} + K_8\phi_{PPC})\eta_o + K_6\eta_4}{i\omega A_5 + K_6 + K_7 + K_8}$$

The resulting expressions include all the sub-embayment and offshore exchanges under the same assumptions of the Chuang and Swenson (1981) model (e.g., no local influences, no overtopping).

4.2 Local Wind Impact on Bay Model

15   The contribution of local wind setup to the spatial distribution of water level inside the bay can be approximated following Wong and Moses-Hall (1998). The bay can be assumed to be a simple long well-mixed embayment for which the cross-bay

gradients and vertical stratification can be ignored. The linearized vertically integrated momentum and mass conservation equations are:

$$\frac{\partial U}{\partial t} = -gh\frac{\partial \eta}{\partial x} + \frac{1}{\rho_0}(\tau_s - \tau_b) = -gh\frac{\partial \eta}{\partial x} + \tau_w - r\frac{U}{h}$$

and

$$\frac{\partial U}{\partial x} = -\frac{\partial \eta}{\partial t}$$

   where η is the water level in the bay; U is the depth integrated along-bay velocity; h is the water depth; τ_s and τ_b are the

5   surface and bottom stresses, respectively; and ρ_0 is the water density. $\tau_w = {\tau_s}/{\rho_0}$ is the spatially invariant wind stress and r

is a linearized bottom friction.

Under the assumption of $\eta = \eta e^{i\omega t}$ and $u = u e^{i\omega t}$, where ω is the angular frequency, the resulting equation is:

$\frac{\partial^2 \eta}{\partial x^2} + \eta\left(\frac{\omega^2}{gh} - \frac{i\omega r}{gh^2}\right) = \frac{\partial^2 \eta}{\partial x^2} + \eta k^2 = 0$ with boundary conditions $\eta(x=0, \omega) = 0$ assuming no offshore forcing at the

entrance (this assumption will be revisited in the next section) and $\frac{\partial \eta(x=L,\omega)}{\partial x} = \frac{\tau_w(\omega)}{gh}$ assuming no flux at the head ($x=L$).

10   The solution is:

$$\eta(\omega) = \frac{\tau_w(\omega)sin(kx)}{ghk\,cos(Lx)}$$

where $k = \left(\frac{\omega^2}{gh} - \frac{i\omega r}{gh^2}\right)^{1/2}$.

4.3 Combining Local and Remote Effects

15   The local and remote effects can be combined in following the approach by Wong and Moses-Hall (1998). The boundary

condition for the local wind effect can be altered to account for the influence of offshore water level, η_o. The resulting model

is a modification of the wind effect model that considers the analytical offshore influence in Section 4.1. In a system with a

single   inlet,   the   solution   can   be   simply   stated   as   in   Wong   and   Moses-Hall   (1998):

$$\eta(\omega) = \frac{\tau_w(\omega)\,sin(kx)}{ghk\,cos(Lx)} + \eta_o(\omega)\frac{cos\big(k(L-x)\big)}{cos(Lx)}$$

In a system with multiple connections with the offshore, the solution can be more complex. One limitation of the approach is

20   that it utilizes a linear friction approximation. To produce a better approximation that takes into account the complex

frictional conditions of the bay (e.g., varying geometry, diverse bottom conditions, enhanced attenuation over submerged

vegetation), we can take a numerical solution of the bay that resolves the tidal and sub-tidal water level conditions under

realistic friction and adjust the spatial distribution of the transfer from offshore accordingly. As most of the water level and

flow variability in the bay is associated with the M_2 semidiurnal tidal constituent (Figure 3) and the distribution of the tide

has been properly validated in the numerical simulations (Defne and Ganju, 2015), we can take the spatial distribution of the M_2 tide as a proxy for the internal frictional effects in the bay. The adjustment is applied to each of the sub-embayments following the expression:

$$\frac{\hat{\eta}_j}{\eta_o}(x,\omega) = 1 - \frac{\left(1 - \frac{\eta_j}{\eta_o}(\omega)\right)\left(1 - \frac{\eta_{M_2}(x)}{\eta_{M_2}(offshore)}\right)}{\left(1 - \frac{\eta_j}{\eta_o}(\omega_{M_2})\right)}$$

5   where $\frac{\eta_j}{\eta_o}(\omega)$ is the transfer coefficient of the sub-embayment i (single value) at frequency ω, $\eta_{M_2}(x)$ is the amplitude of the M_2 tidal fluctuations from the numerical model solution (spatially variable), and $\frac{\hat{\eta}_j}{\eta_o}(x,\omega)$ is the spatially variable adjusted transfer coefficient for sub-embayment j. The resulting adjusted transfer coefficients provide estimates of the spatial changes not only between adjacent sub-embayments but also inside each of the sub-embayments. The local wind effects on bay water level can be added to the impact from offshore fluctuations to obtain a combined local and remote water level
10   response estimate.

5 Results

5.1 Offshore transfer to bay

The maximum energy in water level spectra (Figure 3, Table 2) was associated with the M_2 semidiurnal tidal constituent for the offshore proxies (SH and AC) and at the stations TUC and ETH in the southern part of the BBLEH area. For the
15   locations in Barnegat Bay (WAR, SEH, MAN), maximum energy was in the low frequency band. Large spectral energy also occurred in the other semidiurnal tidal frequencies (S_2 and N_2), the diurnal frequencies (O_1 and K_1), the storm band (periods between 2 and 5 days), and the low frequency band (Table 2). The energy in the remaining bands exhibited average fluctuations less than 0.03 m in size offshore, while in the bay fluctuations were less than 0.01 m.
Transfer functions between Atlantic City (AC) and the five stations inside the bay (Figure 4) for the longest available length
20   of record showed a north to south gradient. The transfer of the offshore fluctuations was 50-80% at periods between 2 and 5 days (storm band) except at Tuckerton (TUC; over 95%). The transfers at diurnal periods were about 35% for the three Barnegat Bay stations (WAR, SEH, MAN), about 45% in Little Egg Harbor (ETH), and 80% in Great Bay (TUC). For frequencies associated with the semidiurnal tides, the transfers were even more attenuated with values about 15% (between 14 and 16%) inside Barnegat, 30-35% at ETH, and 60-70% at TUC. As the numerical model solution was only available for
25   the period March-December 2012, the long-term (2007-2018) transfers were compared with shorter-term observations. The transfers were similar (within the uncertainty envelopes for each station, not shown) for both datasets at most frequencies except at Mantoloking (MAN) that showed enhanced transfers for periods between one and five days in the 2012 record and

at Seaside Heights (SEH), where transfers in the storm band were slightly attenuated during 2012. Transfer estimates using Sandy Hook (SH) as the offshore proxy instead of Atlantic City produced similar results (not shown). The transfer between stations AC and SH on the open coast (proxies for offshore fluctuations) has been shown to be close to one (Wong and Wilson, 1984; Aretxabaleta et al., 2014), confirming that the offshore forcing at all three inlets is about the same.

5   Transfers estimated from the numerical model solution (Figure 5) showed similar magnitudes to the observed transfers (within uncertainty envelopes provided by the Bendat and Piersol (1986) formulation) at most frequencies. The observed and modeled transfer at diurnal and semi-diurnal transfers were similar (within a few percentage points) at all stations except the model overestimated the semidiurnal transfer at TUC. Differences between model and observed estimates at MAN and SEH only were significant at frequencies that contained minimal energy. The model reproduced the enhanced transfer in the storm

10   band at Mantoloking during 2012, suggesting a physical mechanism for the change that the model was able to capture but remains unexplained. The model overestimated the transfer at ETH in the storm band and underestimated the low-frequency transfer at Waretown. The likely cause for some of the discrepancies, especially at low frequencies, is the relatively short length of the available record.

The analytical model of offshore impact that considered five sub-embayments (Section 4.1) was fit to the observed transfers

15   to obtain an estimate of linear friction. The fit considered the unevenly distributed energy spectra (Figure 3) with adjusted weight to the semidiurnal and low-frequency components. The resulting friction was r = 0.021 m/s. The associated frictional adjustment time, $t_{fr} = {}^{h}/{r}$, was about 1-5 minutes depending on the depth of the inlet. The analytical curves (Figure 6) matched the observed transfer function shape at most frequencies. The analytical model with five sub-embayment domains captured the north-south spatial differences in transfer. The analytical model for the central Barnegat Bay sub-embayment

20   (A_3) approximated the transfer estimates from observations at Waretown at most frequencies (less than 5 % in the storm band). The analytical model for Great Bay (A_1) adequately matched observed transfers at Tuckerton at diurnal and semidiurnal frequencies (less than 5 % difference) but underestimated the transfer in the storm band (model estimates about 90%, while observations were above 95%). Meanwhile, the analytical model for Little Egg Harbor (A_2) matched the observed transfers at ETH within the uncertainty envelop, except for a slight under-prediction at diurnal frequencies (less

25   than 5%). The observed transfers at the northern stations (MAN and SEH) were reproduced by the analytical model (A_4, A_5 respectively) at diurnal and semidiurnal tides, but were under-predicted for the higher storm band frequencies (5-10% less transfer in frequencies close to 2-day periods) and over-predicted at low frequencies (about 10% differences). The analytical model was used to explore the effect on transfer of the breach (U_7) at Mantoloking that opened during Hurricane Sandy. The transfers were so minimally affected that the curves are indistinguishable with only a negligible enhancement (<0.2%) in

30   transfer in the northern most sub-embayment (A_5). The breach was too small and shallow for any significant volume transport to occur that would affect the large bay.

5.2 Local Wind Influence

The spectrum of the along-bay component (rotated 20 degrees) of the wind (Figure 7a) from the offshore buoy NDBC 44065 (ten years, 2008-2018) showed high energies in the storm band (2-5 days) and in low frequencies. The largest single peak of energy was associated with 24-hour period oscillations likely associated with sea breeze and matched energy values at 5-day

5 frequencies. There was a small peak at inertial frequencies.

The local wind contribution to water level setup inside the bay was approximated using the Wong and Moses-Hall (1998) approach (Section 4.2). The resulting formulation showed largest setup magnitudes near the head of the bay (e.g., northern part with wind blowing from the south) with a decay as distance from head increased (Figure 7b,c). The magnitude of the setup depended on the magnitude of the linear friction with less setup under stronger friction (Figure 7b,c). The frictional

10 control was less important at higher frequencies (Figure 7c). As frequency increases there was less wind energy (Figure 7a), so the frictional control is mostly important for low frequency and storm band wind fluctuations.

The resulting effect of the wind setup (or set-down) was generally small (less than 0.01 m) for most of the domain (Figure 8). The estimate assumed a linear friction of the same magnitude as in Section 5.1 (r=0.021 m/s). Under persistent wind stress in the along-bay direction, the resulting setups varied depending on the frequency considered. Setup magnitudes of

15 over 0.03 m were estimated for the 5-day period wind (Figure 8c), while under half of that magnitude was achieved for the 2-day persistent wind (Figure 8b), and much smaller water level setup (peak smaller than 0.01 m) was estimated for the sea breeze (Figure 8a). During extreme events like Hurricane Sandy, under intense wind stress, two additional effects should be considered: the depth of the bay increases by the transfer of offshore surge resulting in altered setup response (Section 4.2), and the frictional effect is enhanced (a larger linear friction would be needed) by the presence of wave-induced roughness.

20 ## 6 Discussion

6.1 Spatially Variable Water Level Transfer

Following the approach described in Section 4.3, estimates of spatially variable estimates of water level impact from offshore can be calculated (Figure 9). The M_2 tidal constituent transfer (Figure 9a) showed a large north to south gradient with values going from around 10% in the north to over 80% in the vicinity of Little Egg Inlet. The role of Barnegat Inlet in

25 enhancing tidal transfer was greatly reduced as most of the tide was attenuated in the inlet. The contribution of Point Pleasant Canal was also small as expected from the tidal amplitudes (Chant, 2001; Defne and Ganju, 2015). The transfer in the storm band of 2-day fluctuations (Figure 9b) also showed a strong north-south gradient with values about 50% in Barnegat Bay, around 70-80% in Little Egg Harbor and larger values in Great Bay. The 5-day offshore fluctuations were transferred more efficiently into the bay (Figure 9c) with values over 70% in the entire bay, reaching 80-90% in Little Egg

30 Harbor, and over 90% in Great Bay. Both storm band transfer estimates were controlled by the exchange through Little Egg

Inlet, with very local transfer enhancements in the vicinity of Barnegat Inlet and Point Pleasant Canal. While the presented estimates used Atlantic City as offshore proxy, similar results were obtained when Sandy Hook was used as the offshore reference (as expected from Aretxabaleta et al., 2014).

When the magnitude of the fluctuations associated with a specific storm are available η_o, then an estimate of the average
5 water level in the bay during the storm can be obtained. For instance, for Hurricane Sandy the offshore surge associated with the storm was of the order of 2-3 m. Considering that the storm lasted for over a day, the water level transfer would have been above 50% in Barnegat Bay and above 70% in Little Egg Harbor. The resulting surge estimate in the bay was between 1 and 2 m just considering the exchange through the existing inlets. There was reported overtopping of the barrier island during the storm (McKenna et al., 2016) that might have further increased water level in the bay that the proposed method
10 does not consider.

The wind setup effect inside the bay due to local wind can also be estimated for Hurricane Sandy using the approach in Section 4.2. Maximum wind stress during the storm was about 1 Pa. To obtain a maximum effect (worst-case scenario) the wind was assumed to be persistently in the along-bay direction and that maximum stress was maintained for the duration of the storm. The maximum resulting water level considering the Wong and Moses-Hall method is linear with regard to wind
15 stress magnitude (Figure 7b) would have been 10 times larger than the setup in Figure 8b. The maximum setup would have been about 0.2 m, which was 5-10 times smaller than the surge produced from offshore sources. The cross-bay contribution to the wind setup during Sandy was comparatively small as wind direction was predominantly along-bay.

6.2 Transfer Based on Tidal Database

The approach this far was based on the combination of observations, analytical models and numerical models. In many
20 systems, long-term observations that allow for the estimation of transfer coefficients might not be available. Also, numerical solutions of back-barrier bay systems tend to be computationally expensive and might not be available for the period of interest. We propose a relatively simpler approach for some of these systems based on the availability of high-resolution tidal solutions for the system. The EC2015 ADCIRC tidal database (Szpilka et al., 2016) showed sufficient resolution (down to 13m in some areas) in many bays along the east coast of the United States to resolve the tidal conditions with skill when
25 compared to NOAA CO-OPS stations and historic International Hydrographic Organization (IHO) data. The EC2015 tidal database provides estimates for 37 tidal constituents. Based on those constituents and assuming that the totality of the offshore fluctuations at zero frequency reach the interior of the bay, an estimate can be provided for the storm band frequencies. A weighted least squares interpolation in the frequency domain was performed based on the M_4, K_2, S_2, L_2, M_2, N_2, K_1, P_1, O_1, Q_1 tidal amplitudes ratios between each point of the ADCIRC domain inside the bay and a point in the
30 offshore. Higher weight was given to zero frequency to nudge toward 100% transfer at zero frequency. Estimates were calculated based on multiple locations inside the bay and average to achieve a more robust calculation and also obtain an approximation to the uncertainty associated with the estimate.

The resulting transfer estimates (Figure 10) exhibited the same general spatial patterns shown in the previous estimates (Figure 9) with slight differences. Some of the smaller features present in the COAWST numerical solution (Defne and Ganju, 2015) were not present in the ADCIRC EC2015 domain. The M_2 transfer estimate based on the tidal database (Figure 10a) presented approximately the same magnitudes in most areas (average difference less than 3%). The 5-day transfer

5 (Figure 10c) was also comparable to the solution described in Section 6.1 with values over 70% in the entire domain and the southern areas exceeding 90% transfer. The 2-day transfer from ADCIRC (Figure 10b) was 5-10% higher than the direct estimates (Figure 9b). One of the benefits of the ADCIRC approach was the possibility of providing an approximation to the uncertainty (Figure 11). The uncertainty estimate of the M_2 transfer was about 1-2% (Figure 11a) with higher values in the southern part of the domain. The 2-day transfer uncertainty (Figure 11b) was above 4% in Barnegat Bay in areas of larger

10 discrepancy between the ADCIRC and complete approaches. The uncertainty estimates in the 5-day transfer (Figure 11c) in the northern part of the domain did not exceed 2.5%.

The magnitude of the difference between the ADCIRC tidal database approach and the complete method highlighted in Section 4.3 was of the same order of magnitude or even smaller than the difference between observations and analytical model (Figure 6) or between observed and numerical modeled transfers (Figure 5). This result emphasizes the validity of

15 using the tidal database to calculate transfer estimates, especially when water level observations inside the bay or numerical solutions are not available.

6.3 Validity for Flooding Hazard Assessments

The method presented offers a new methodology for coastal hazards assessment and risk analysis. While many methodologies are being used for open-coast regions (Thieler and Hammar-Klose, 1999; Kunreuther et al., 2000),

20 vulnerability evaluation to coastal hazards in back-barrier bays remains under developed. Evaluating bay hazards usually requires expensive computational simulations at appropriate high resolutions to characterize the spatial and temporal effects. The method presented here, using existing ADCIRC results, provides a less expensive approach that is able to properly estimate the spatial differences in vulnerability in response to flooding at different time scales (e.g., perigean spring tides, storms of different duration). It provides guidance for planning in response to "nuisance" flooding at a relatively low cost. It

25 can be expanded to all back-barriers without the need to simulate each storm in each embayment, while applying a consistent methodology.

As part of the general needs for hazard assessment (Ludwig et al., 2018), the important hazard characteristics that decision makers require include spatial extent, duration, and magnitude. The proposed methodology provides an approximation to both the area extent and magnitude, and also variations based on storm duration. Additionally, the fact that uncertainty

30 estimates accompany the vulnerability provided by the present method enhances the potential value to decision makers. The extension to other bays in the United States will be included as part of the U. S. Geological Survey Coastal Change Hazards portal (USGS, 2018).

7 Summary

The results presented here demonstrate a strategy for estimating the impact of offshore sea level and local wind setup in back-barrier bay water levels. The transfer estimates of offshore to bay water level used a combination of observations, analytical models based on appropriate simplifications of the bay system, and numerical simulations that provide the needed
5 spatial distribution and more realistic frictional control.

The resulting maps of water level response to offshore forcing showed larger attenuation of the relatively higher frequency fluctuations such as the semidiurnal tides. Smaller transfers were associated with shorter duration storms than longer duration storms and transfer was most spatially uniform for storms of long duration. The description of the magnitude and spatial dependence of transfer on storm duration will assist planning for flooding in back-barrier bays.

10 In the specific case of the Barnegat Bay-Little Egg Harbor system, larger transfers were estimated for the southern embayments (Great Bay and Little Egg Harbor) when compared to Barnegat Bay. The reason for the difference was the dominant role of Little Egg Inlet (wider and deeper) in controlling the exchange between the offshore and bay systems. The contribution of local wind to bay water level setup was much smaller, but not negligible, compared to the transfer from offshore fluctuations.

15 We introduced two approaches depending on the availability of observations and numerical solutions. The less data-requiring approach based on the ADCIRC tidal database provides spatial transfer estimates and measures of uncertainty. The approach that includes an analytical model allows for a simple tool to study the response of back-barrier bay systems to alternative conditions and forcing (e.g., geomorphic changes, changing duration of storms, sea level rise).

The proposed method represents an effective and inexpensive approach to flooding hazard evaluation in back-barrier bays
20 and inland waters. The method provides detailed spatial estimates of vulnerabilities and uncertainties that could be an intuitive tool for coastal managers.

Author Contribution

A.L. Aretxabaleta developed the methodology and wrote most of the manuscript. N.K. Ganju and R.P. Signell suggested improvements to the methodology. Z. Defne contributed to the figure generation, the COAWST simulation analysis, and the
25 discussion of results. All authors contributed to the final version.

Competing Interests

The authors declare that they have no conflict of interest.

Disclaimer

This draft manuscript is distributed solely for purposes of scientific peer review. Its content is deliberative and pre-decisional, so it must not be disclosed or released by reviewers. Because the manuscript has not yet been approved for publication by the U.S. Geological Survey (USGS), it does not represent any official USGS finding or policy. Use of firm and product names is for descriptive purposes only and does not imply endorsement by the U.S. Government.

Acknowledgments

The authors thank Brad Butman for helpful comments on the manuscript. This work was supported by the U.S. Geological Survey, Coastal and Marine Hazards/Resources Program. The hydrodynamic model outputs used in this study are available at http://geoport.whoi.edu/thredds/dodsC/sand/usgs/users/zdefne/run0x, where x stands for the run number. The numerical model is the open source model COAWST available from https://coawstmodel-trac.sourcerepo.com after registration with J. C. Warner (jcwarner@usgs.gov) at the U.S. Geological Survey. The data used are listed in the references, tables, and the repository at http://waterdata.usgs.gov/nwis/inventory/?site_no=xxx, where xxx stands for the USGS station number in Table 1. The paper benefited from conversations with Chris Sherwood, Tarandeep Kalra, and John Warner from USGS.

References

Aretxabaleta, A. L., Butman, B., and Ganju, N. K.: Water level response in back-barrier bays unchanged following Hurricane Sandy, Geophys. Res. Lett., 41, 9, 3163–3171, doi:10.1002/2014GL059957, 2014.

Aretxabaleta, A. L., Ganju, N. K., Butman, B., and Signell, R. P.: Observations and a linear model of water level in an interconnected inlet- bay system, J. Geophys. Res., 122, doi:10.1002/2016JC012318, 2017.

Bendat, J. S., and Piersol, A. G.: Random data. Analysis and measurement procedures, 566 pp., John Wiley & Sons, New York, 1986.

Chant, R. J.: Tidal and subtidal motion in a shallow bar-built multiple inlet/bay system, J. Coast. Res., 32(Special Issue), 102-114, 2001.

Chuang, W.-S., and Swenson, E. M.: Subtidal Water level variations in Lake Pontchartrain, Louisiana, J. Geophys. Res., 86(C5), 4198–4204, doi:10.1029/JC086iC05p04198, 1981.

Defne, Z., and Ganju, N. K.: Quantifying the Residence Time and Flushing Characteristics of a Shallow, Back-Barrier Estuary: Application of Hydrodynamic and Particle Tracking Models, Estuaries and Coasts, 38, 1719–1734, doi: 10.1007/s12237-014-9885-3, 2015.

Garvine, R. W.: A simple model of estuarine subtidal fluctuations forced by local and remote wind stress, J. Geophys. Res., 90(C6), 11,945–11,948, 1985.

Janzen, C. D., and Wong, K.-C.: Wind-forced dynamics at the estuary-shelf interface of a large coastal plain estuary, J. Geophys. Res., 107(C10), 3138, doi:10.1029/2001JC000959, 2002.

Keulegan, G. H.: Tidal flow in entrances: water-level fluctuations of basins in communication with seas, Committee on Tidal Hydraulics, Technical Bulletin No. 14, U.S. Army Corps of Engineers, Vicksburg, Miss., 89 pp., 1967.

5 Klein, R.J. and Nicholls, R. J.: Assessment of coastal vulnerability to climate change, Ambio, 182-187, 1999.

Kunreuther, H., Platt, R., Baruch, S., Bernknopf, R. L., Buckley, M., Burkett, V., Conrad, D., Davidson, T., Deutsch, K., Geis, D., and Jannereth, M.: The hidden costs of coastal hazards: Implications for risk assessment and mitigation, H. John Heinz III Center for Science, Economics, and the Environment. Panel on Risk, Vulnerability, and the True Costs of Coastal Hazards and H. John Heinz III Center for Science, Economics, and the Environment, 220 pp., Island Press, Washington, D.

10 C., 2000.

Ludwig, K. A., Ramsey, D. W., Wood, N. J., Pennaz, A. B., Godt, J. W., Plant, N. G., Luco, N., Koenig, T. A., Hudnut, K. W., Davis, D. K., and Bright, P. R.: Science for a risky world—A U.S. Geological Survey plan for risk research and applications: U.S. Geological Survey Circular 1444, 57 pp., https://doi.org/10.3133/cir1444, 2018.

McKenna, K. K., Farrell, S. C., and Gebert, J. A.: Hurricane Sandy: Beach-dune recovery at New Jersey Beach Profile

15 Network (NJBPN) sites, Shore & Beach, 84(3), 5-17, 2016.

Nicholls, R.J., Wong, P. P., Burkett, V. R., Codignotto, J. O., Hay, J. E., McLean, R. F., Ragoonaden, S., and Woodroffe, C. D.: Coastal systems and low-lying areas. Climate Change 2007: Impacts, Adaptation and Vulnerability. Contribution of Working Group II to the Fourth Assessment Report of the Intergovernmental Panel on Climate Change, Parry, M. L., Canziani, O. F., Palutikof, J. P., van der Linden, P. J., and Hanson, C. E., Eds., Cambridge University Press, Cambridge, UK,

20 315-356, 2007.

Szpilka, C., Dresback, K., Kolar, R., Feyen, J., and Wang, J.: Improvements for the Western North Atlantic, Caribbean and Gulf of Mexico ADCIRC Tidal Database (EC2015), J. Mar. Sci. Eng, 4(4), p.72, doi:10.3390/jmse4040072, 2016.

Thieler, E. R., and Hammar-Klose, E. S.: National Assessment of Coastal Vulnerability to Sea-Level Rise: Preliminary Results for the US Atlantic Coast, Woods Hole, MA: United States Geological Survey (USGS), Open File Report 99-593,

25 1999.

U.S. Geological Survey, 2018, Coastal Change Hazards Portal web page, accessed October 30, 2018, at http://marine.usgs.gov/coastalchangehazardsportal/.

Warner J. C., Armstrong, B., He, R., and Zambon, J. B.: Development of a Coupled Ocean–Atmosphere–Wave–Sediment Transport (COAWST) Modeling System, Ocean Modelling, 35, 230-244, doi: 10.1016/j.ocemod.2010.07.010, 2010.

30 Wilkin, J. L., and Hunter, E. J.: An assessment of the skill of real-time models of Mid-Atlantic Bight continental shelf circulation, J. Geophys. Res., 118 (6), 2919-2933, 2013.

Wong, K.-C., and DiLorenzo, J.: The response of Delaware's inland bays to ocean forcing, J. Geophys. Res., 93(C10), 12525–12535, 1988.

Wong, K.-C., and Moses-Hall, J. E.: On the relative importance of the remote and local wind effects to the subtidal variability in a coastal plain estuary, J. Geophys. Res., 103(C9), 18393–18404, 1998.

Wong, K.-C., and Wilson, R. E.: Observations of low-frequency variability in Great South Bay and relations to atmospheric forcing, J. Phys. Oceanogr., 14, 1893–1900, 1984.
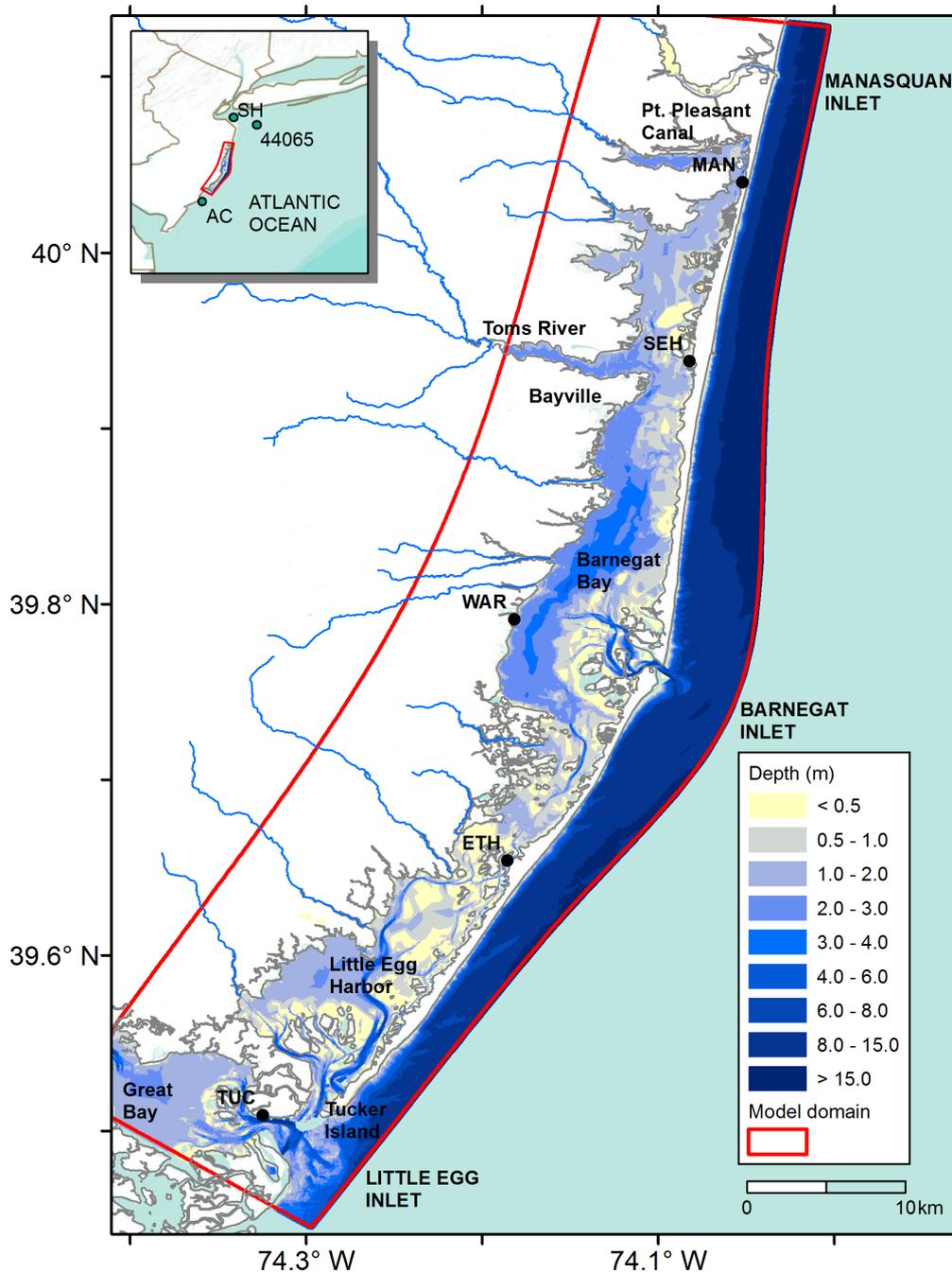
Figure 1. Map of Barnegat Bay and Little Egg Harbor estuary showing the water level stations, bays, and inlets. The water level stations are: Tucketon (TUC); East Thorofare (ETH); Waretown (WAR); Seaside Heights (SEH); and Mantoloking (MAN). Locations of offshore water level proxy stations and wind buoy are indicated in inset. COAWST model domain boundary is shown in red. Rte. 72 crosses the bay near ETH station and the breach that occurred during Hurricane Sandy was about a hundred
5   meters away from MAN station, so they are not indicated in the map.
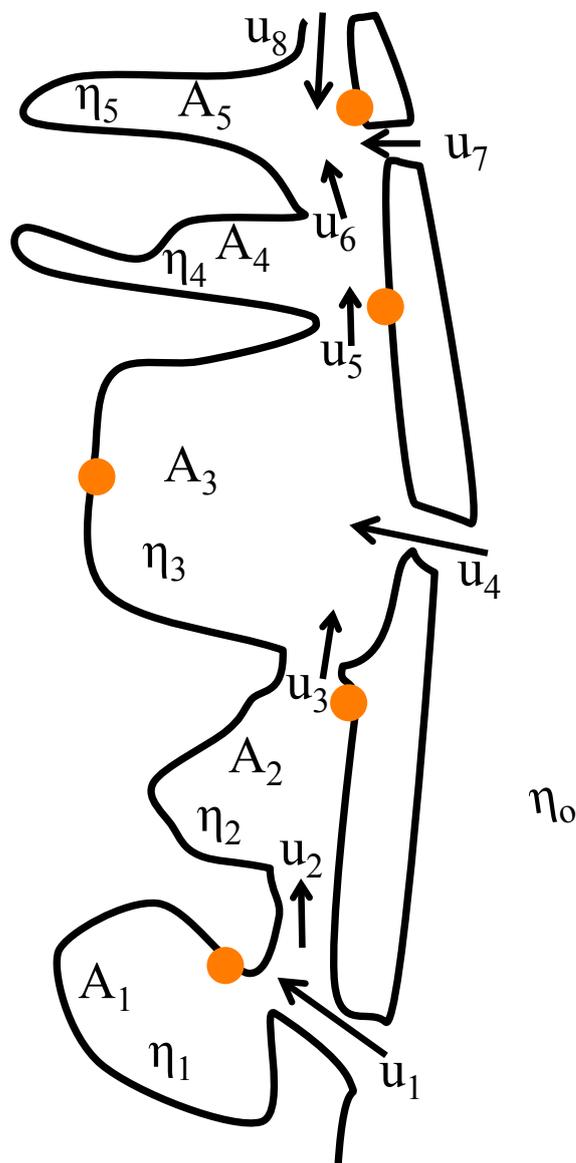
Figure 2. Schematic diagram of the ocean-inlet-bay system: A_j is the surface area of the bays; η_j the sea level in the bays; η_o the sea level in the ocean; and u_j is the velocity through channel j. The correspondence with the real bay system includes

areas from the bays (Great Bay, A_1; Little Egg Harbor, A_2; Barnegat Bay, A_3; Toms River sub-embayment, A_4; North of Mantoloking, A_5), flow through inlets (Little Egg Inlet, u_1; Barnegat Inlet, u_4; Point Pleasant Canal, u_8; and Mantoloking breach, u_7), and flow between bays (Tucker Island, u_2; Route 72, u_3; Bayville, u_5; Mantoloking, u_6). The location of the water level stations are indicated with dots and the names and specifications are in Figure 1 and Table 1.
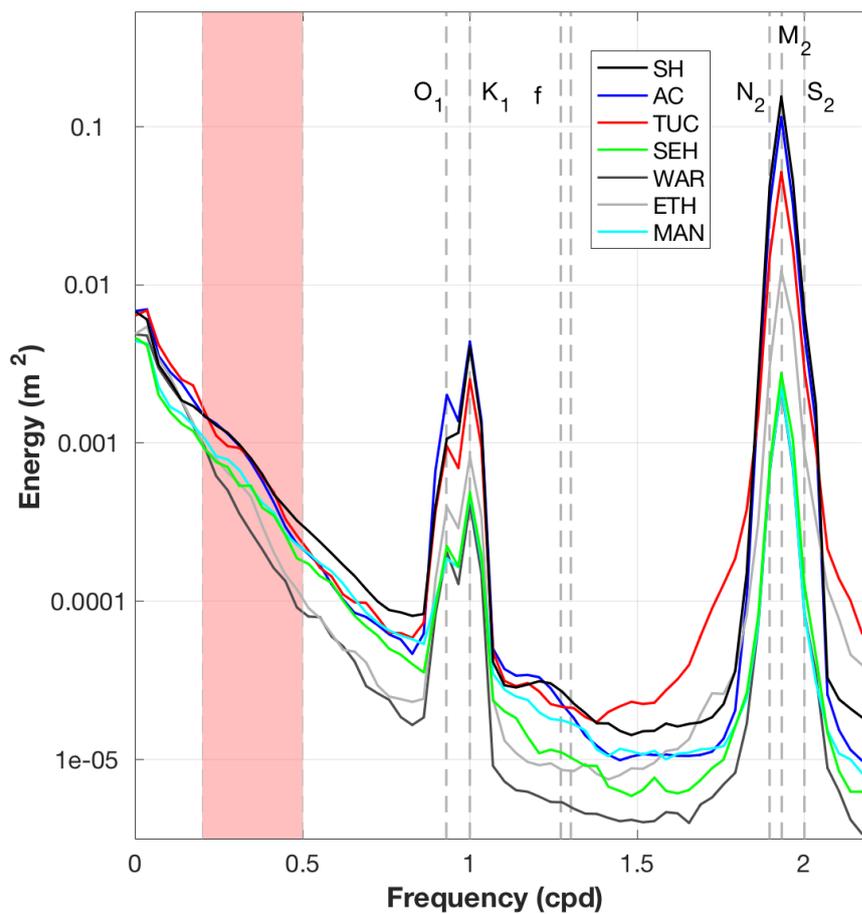
Figure 3. Energy spectra at all stations computed using a Hanning 29-day window with over-lapping (50%) data segments. O₁, K₁, N₂, M₂, and S₂ label the principal tidal frequencies and _f_ the inertial frequency. The vertical shaded area indicates the frequencies corresponding to the storm band (2-5 days). (cpd: cycles per day). See Table 1 for key to station abbreviations and Figure 1 for locations.
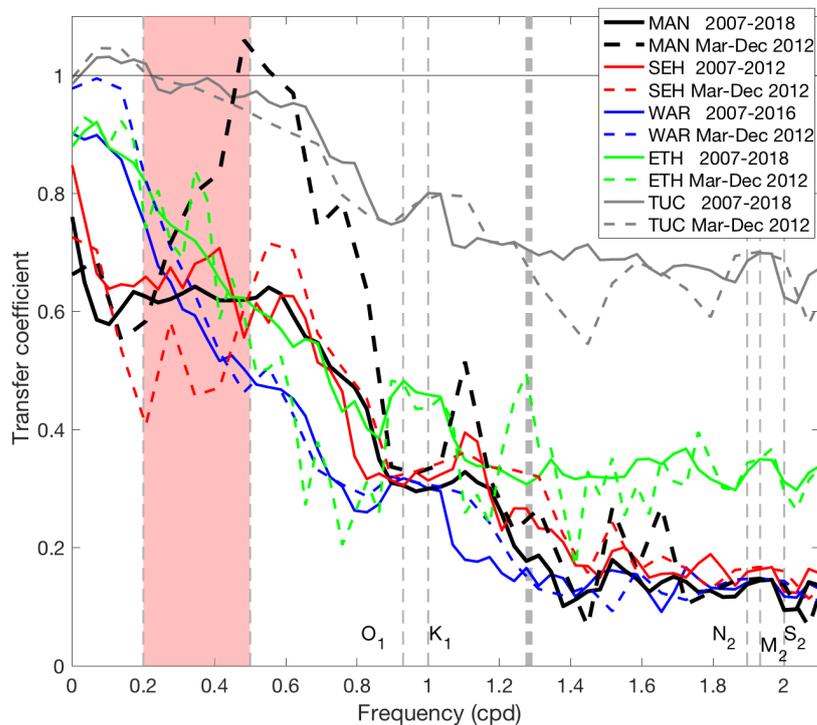
Figure 4. Observed transfer from Atlantic City to 5 bay stations: Mantoloking (MAN), Seaside Heights (SEH), Waretown (WAR), East Thorofare (ETH), and Tuckerton (TUC). Solid lines indicate transfers for the entire available record at each station. Dashed lines represent observed transfers for the period March-December 2012, for which numerical model solutions were available. The vertical shaded area indicates the frequencies corresponding to the storm band (2-5 days).
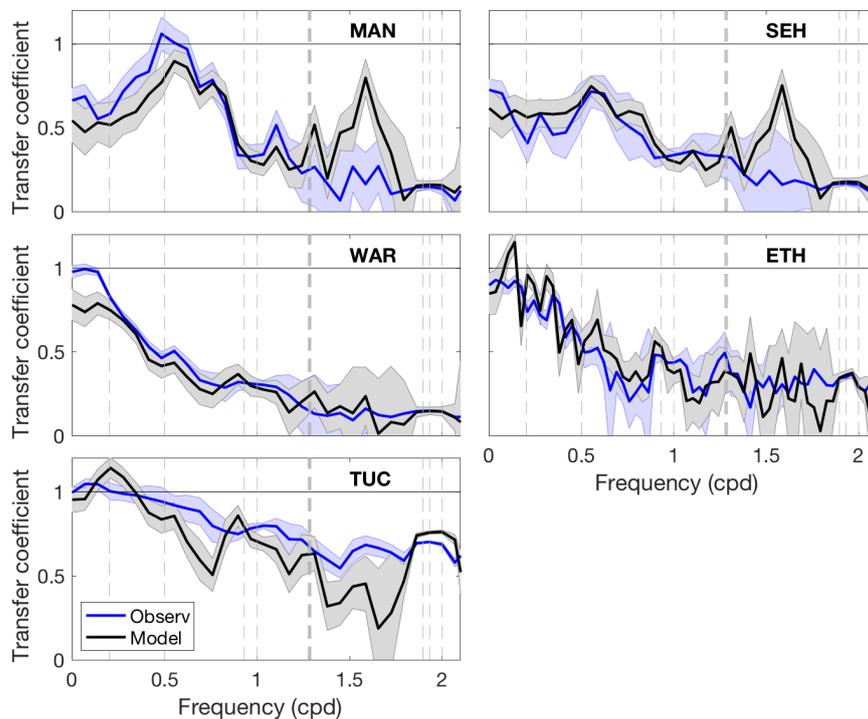
Figure 5. Comparison between observed (blue) and numerical model (black) transfers for the period when both are available (March-December 2012) at five bay stations. Uncertainty envelopes for the transfer coefficient (Bendat and Piersol, 1986) are provided for observed (light blue) and model (gray) estimates.
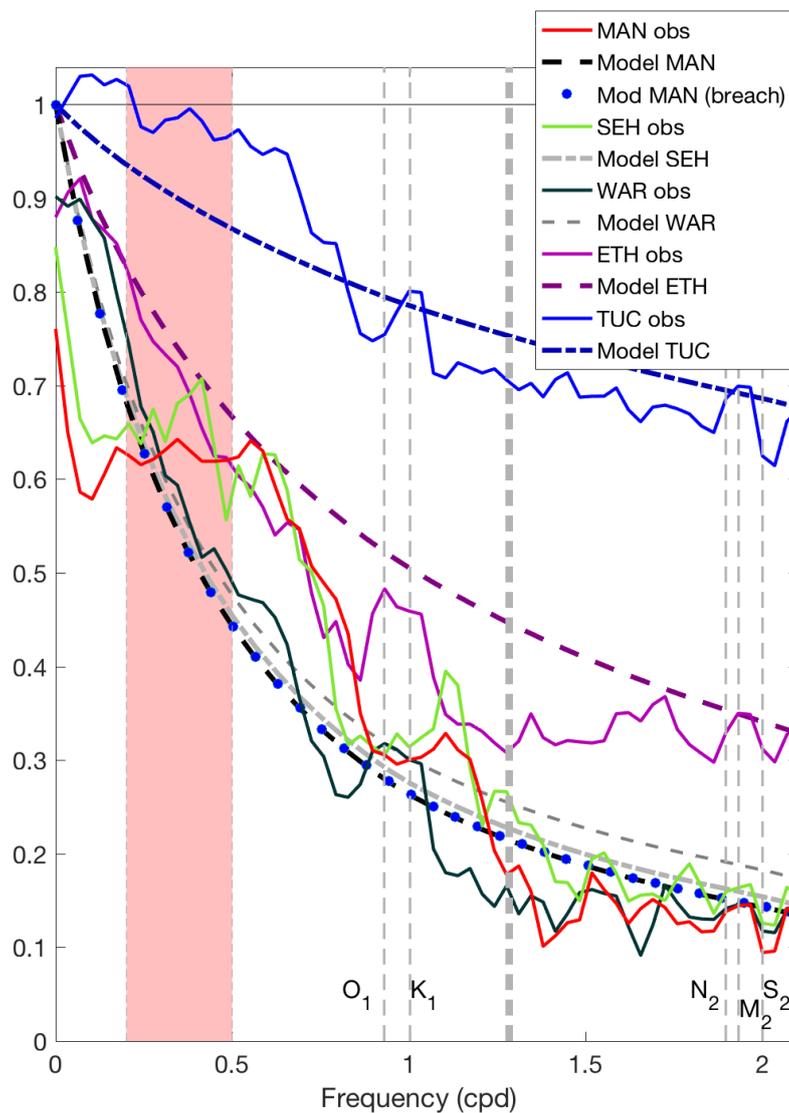
Figure 6. Observed transfer for longest available record (solid lines) and best analytical model fit for each of the sub-embayments (dashed lines). The vertical shaded area indicates the frequencies corresponding to the storm band (2-5 days).
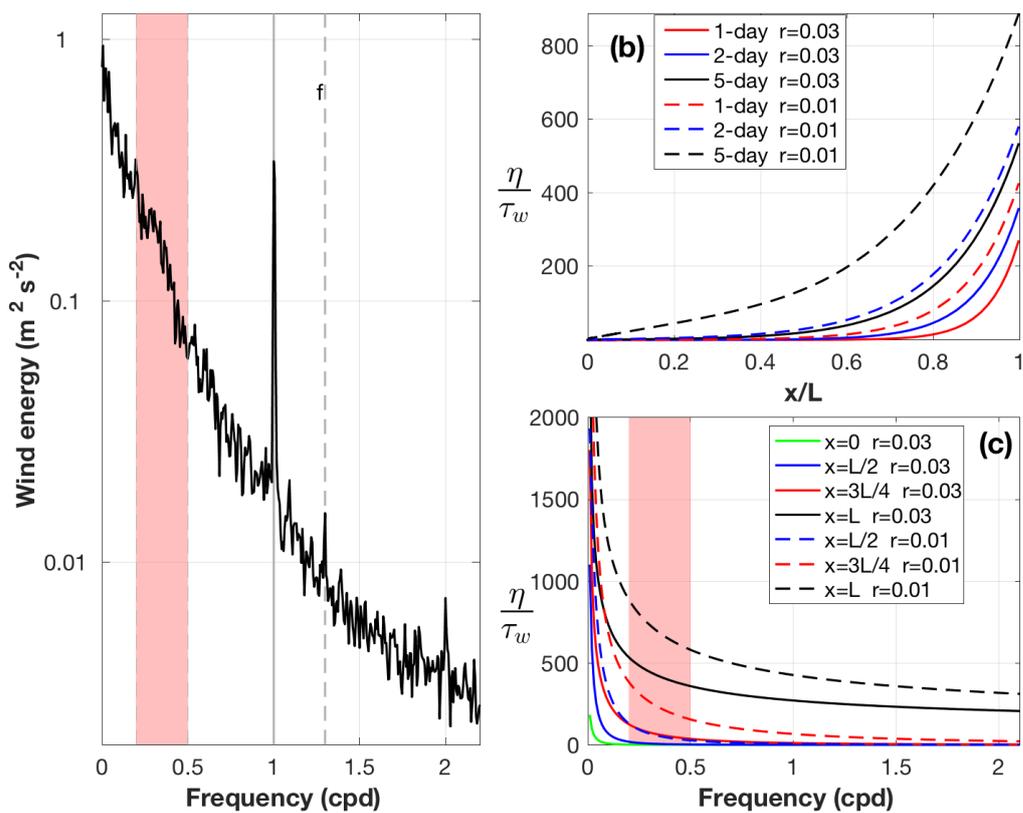
Figure 7: (a) Wind stress spectra for the along-bay wind component for NDBC 44065 buoy (2008-2018). (b) Wind stress contribution to local water level in the bay expressed as η/τ_w (m⁻¹s²) following the Wong and Moses-Hall (1998) formulation as a function of distance from the southern edge of the bay. (c) Wind stress contribution to water level as a function of frequency. The vertical shaded area indicates the frequencies corresponding to the storm band (2-5 days).
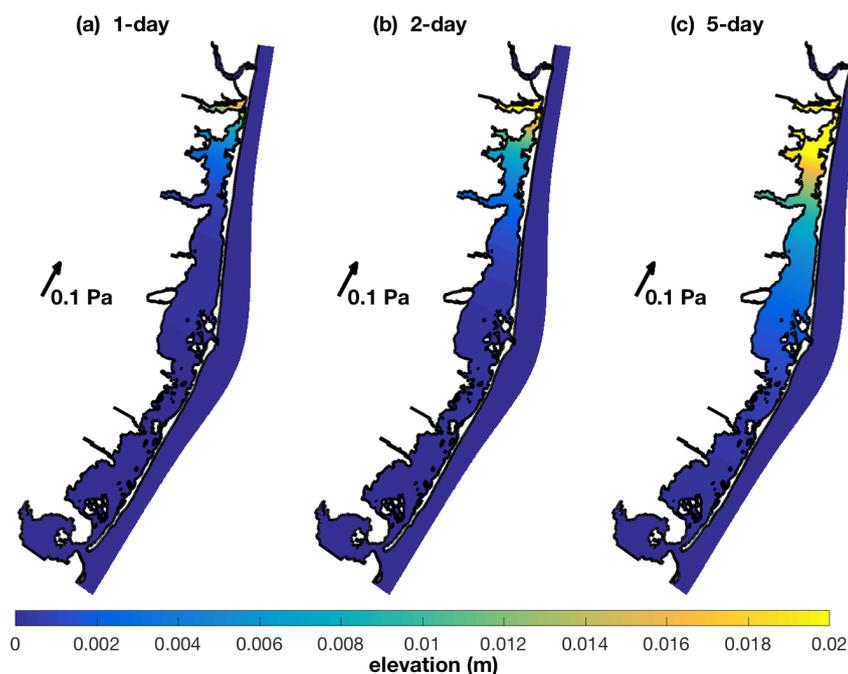
Figure 8: Local wind setup inside the bay based on the Wong and Moses-Hall (1998) formulation for a wind stress of 0.1 Pa at specific periods: (a) wind with a 1-day period (e.g., sea breeze); (b) 2-day wind; and (c) 5-day wind.
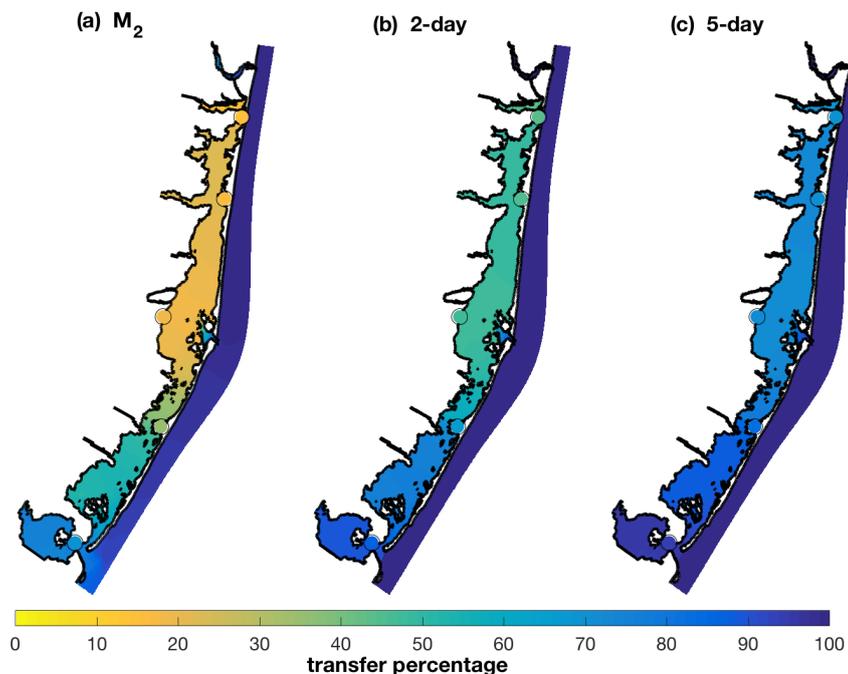
Figure 9. Spatially variable transfer function (percentage) of offshore fluctuations transferred into the bays using Atlantic City as offshore proxy for three frequencies: (a) M_2 semidiurnal tide; (b) 2-day fluctuation in the storm band; and (c) 5-day fluctuation in the storm band. The filled circles represent the transfer estimate at each of the observed locations. Spatial pattern computed using the COAWST numerical solution.
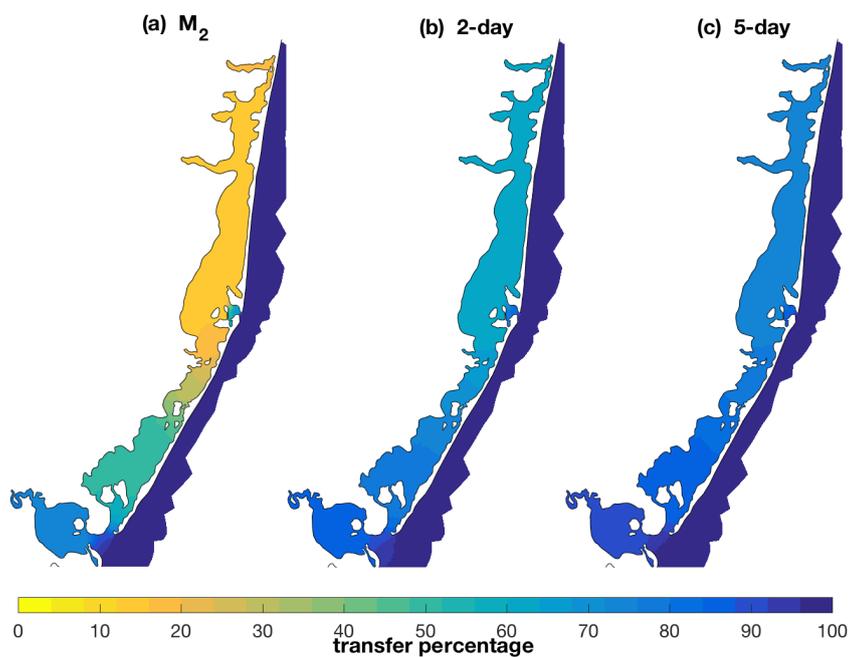
Figure 10: Transfer estimate based on ADCIRC tidal database for three frequencies: (a) M2 semidiurnal tide; (b) 2-day fluctuation in the storm band; and (c) 5-day fluctuation in the storm band.
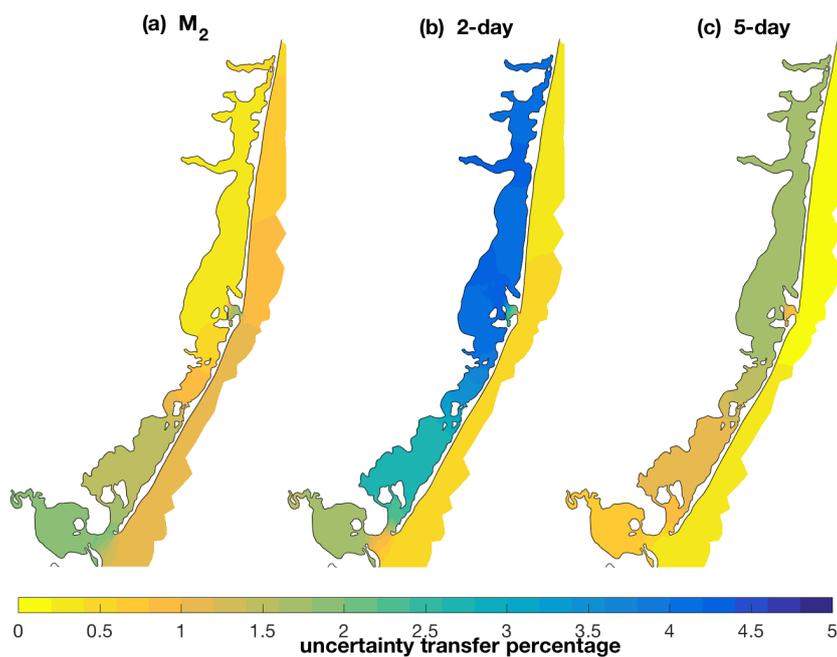
Figure 11: Uncertainty in transfer estimate based on ADCIRC tidal database for three frequencies: (a) M2 semidiurnal tide; (b) 2-day fluctuation in the storm band; and (c) 5-day fluctuation in the storm band.

Table 1. Sites used in water level analysis. Check Figure 1 for locations. National Oceanic and Atmospheric Administration (NOAA); U.S. Geological Survey (USGS). Information on instrumentation type, sampling and quality control methodologies from the USGS stations is available in water.usgs.gov.

Site name (Abbreviation)	Operator/ Site ID	Inlet/Bay	Available Period	Datum	Adjustment to NAVD88
Sandy Hook, NJ (SH)	NOAA 8531680	Offshore proxy	Jan 1910 – May 2018	MSL	0.15 m
Atlantic City, NJ (AC)	NOAA 8534720	Offshore proxy	Aug 1911 – May 2018	MSL	0.12 m
Barnegat Bay at Mantoloking (MAN)	USGS 01408168	Barnegat Bay	Oct 2007- May 2018	NGVD29	0.34 m
Barnegat Bay at Seaside Heights (SEH)	USGS 01408750	Barnegat Bay	Oct 2007- Oct 2012	NGVD29	0.35 m
Barnegat Bay at Waretown (WAR)	USGS 01409110	Barnegat Bay	Oct 2007- Dec 2016	NGVD29	0.37 m
East Thorofare at Ship Bottom (ETH)	USGS 01409146	Little Egg Harbor	Oct 2007- May 2018	NGVD29	0.38 m
Little Egg Inlet near Tuckerton (TUC)	USGS 01409335	Great Bay	Oct 2007- May 2018	NGVD29	0.38 m

5   **Table 2. Sum of energy (m^2) in the different bands of the spectra computed for the period 2007-2018 (or longest available record) using a 29-day Hanning window with over-lapping (50%) data segments.**

Site	Low frequency	2-5 days	1-2 days	Diurnal tide	0.5-1 days	Semidiurnal tide	High frequency
SH	0.023	0.007	0.002	0.008	0.001	0.251	0.002
AC	0.025	0.007	0.001	0.010	0.001	0.187	0.001
TUC	0.025	0.006	0.001	0.005	0.001	0.090	0.001

ETH	0.020	0.004	0.001	0.002	<0.001	0.023	0.001
WAR	0.019	0.003	0.001	0.001	<0.001	0.004	<0.001
SEH	0.015	0.004	0.001	0.001	<0.001	0.005	<0.001
MAN	0.015	0.005	0.001	0.001	<0.001	0.004	<0.001